LITHOGRAPHY

Direct optical lithography of functional inorganic nanomaterials

Yuanyuan Wang,[1,2] Igor Fedin,[1,2] Hao Zhang,[1,2] Dmitri V. Talapin[1,2,3]*

Photolithography is an important manufacturing process that relies on using photoresists, typically polymer formulations, that change solubility when illuminated with ultraviolet light. Here, we introduce a general chemical approach for photoresist-free, direct optical lithography of functional inorganic nanomaterials. The patterned materials can be metals, semiconductors, oxides, magnetic, or rare earth compositions. No organic impurities are present in the patterned layers, which helps achieve good electronic and optical properties. The conductivity, carrier mobility, dielectric, and luminescence properties of optically patterned layers are on par with the properties of state-of-the-art solution-processed materials. The ability to directly pattern all-inorganic layers by using a light exposure dose comparable with that of organic photoresists provides an alternate route for thin-film device manufacturing.

Solution-processed colloidal nanocrystals (NCs) and quantum dots (QDs) have emerged as a versatile platform for building electronic and optoelectronic devices (*1*). These materials enable nonepitaxial deposition and low-temperature processing of, for example, light-emitting diodes (LEDs), field effect transistors (FETs), near- and mid-infrared photodetectors, and solar cells. The transition from individual devices to the level of electronic circuits, sensor arrays, and high-definition QD LED displays requires development of material-adapted patterning methods. Depending on the resolution, throughput, and defect tolerance, various patterning and deposition techniques can be considered, including photolithography and imprint lithography, microcontact and inkjet printing, and laser or electron beam (e-beam) writing (*2*). Among these, photolithography evolves as a method of choice for the electronics industry because of the combination of high resolution and very low cost per patterned element (*3*). The latter comes from the parallel nature of the lithographic process; billions of circuit elements can be defined simultaneously, in contrast to serial techniques such as inkjet printing and e-beam writing.

We demonstrate a method that we call direct optical lithography of functional inorganic nanomaterials (DOLFIN). This process combines multiple benefits of traditional photolithography and is tailored toward efficient patterning of inorganic nanomaterials and sol-gel chemicals without diluting or contaminating them with organic photoresists and other by-products. Almost any inorganic functional material can be prepared in the form of NCs by using a variety of available solution- and gas-phase techniques. Atoms at NC surfaces easily engage in chemical bonding with molecular species—so-called surface ligands—that provide colloidal stability to NCs in desired solvents (*4*). The ligand molecules can be constructed as ion pairs, Cat^+X^-, where X^- is an electron-rich nucleophilic group that binds to the electron-deficient (Lewis acidic) surface sites, typically metal ions. The negative charge on X^- is balanced by a cation, Cat^+, as shown in Fig. 1A. In polar solvents, cations dissociate from the surface and form an ionic cloud responsible for colloidal stabilization, whereas in nonpolar environments or in films, the ion pairs stay tightly bound (*5*).

To implement DOLFIN, we designed photochemically active X^- and Cat^+ groups to enable direct optical patterning of all-inorganic NCs. In one approach, diphenyliodonium (Ph_2I^+) or triphenylsulfonium (Ph_3S^+) cations, also known as photoacid generators (PAGs) (*3*), were combined with surface-binding inorganic anions, such as $Sn_2S_6^{4-}$, $CdCl_4^{2-}$, or MoO_4^{2-} (Fig. 1B). Such ligands provide colloidal stability to metals, semiconductors, and many other types of NCs (fig. S1). Upon photon absorption, PAG molecules decompose, releasing acidic protons (Fig. 1B). These protons can react with the X^- group or with the NC surface in several different ways that alter NC solubility in polar and nonpolar solvents (*6*). As an alternative approach, the X^- group itself can be made photosensitive, as in the case of ammonium 1,2,3,4-thiatriazole-5-thiolate ($NH_4CS_2N_3$, or TTT). The $CS_2N_3^-$ group photochemically decomposes to surface-bound SCN^- ions, N_2, and sulfur (Fig. 1, B and C) (*7*). The ligands with PAG^+ or $CS_2N_3^-$ fragments nicely complement each other: PAG-based ligands are extremely flexible and versatile, whereas TTT ligands can be used with pH-sensitive materials.

The photoactive anionic or cationic ligand components show strong UV absorption bands that can impose on top of the absorption spectra of corresponding NCs, as in the case of CdSe QDs with TTT ligands (Fig. 1C). These ligands provide excellent colloidal stability in N,N-dimethylformamide (DMF), dimethylsulfoxide (DMSO), and other conventional solvents (Fig. 1D and fig. S2). However, irradiation with UV light ($\lambda < 360$ nm) triggers decomposition of TTT ligands, making the NCs insoluble in DMF. The photochemical transformation of $CS_2N_3^-$ to SCN^- can be traced by using characteristic IR absorption features of the $CS_2N_3^-$ and SCN^- groups shown in Fig. 1C, inset, and fig. S3. Various patterns can be generated on rigid and flexible substrates by illuminating NC films through a mask and then washing off the unexposed NCs with DMF (Fig. 1, E and F, and fig. S4). We observed a clear loss of colloidal stability after exposing the NC films to 254 nm, 6.3 mW/cm^2 light for 20 s, which corresponds to an exposure dose of 120 mJ cm^{-2}. For reference, conventional organic photoresists (such as Shipley S1800 series, Dow Chemicals) require a comparable 80 to 150 mJ cm^{-2} exposure dose (*6*). Similarly, NCs with PAG-based ligands were patterned by using a 40 to 70 mJ cm^{-2} exposure dose (fig. S5). Moreover, PAGs can be engineered to operate in different spectral regions, ranging from the deep UV to the visible (fig. S6). The decomposition of surface ligands does not cause changes in the size or shape of NCs, as demonstrated by the unaltered absorption spectra (Fig. 1C), scanning electron microscopy (SEM) (figs. S7 and S8), transmission electron microscopy (fig. S9), and x-ray diffraction patterns (fig. S10). After the first layer was patterned, we repeated the process to create multilayer patterns—for example, patterns of red (R)–, green (G)–, and blue-emitting (B) QDs (Fig. 1E). Complex patterns—such as the one in Fig. 1F, which is composed of ~0.8 million RGB subpixels—can be generated in three DOLFIN steps because of the parallel patterning of many elements.

Both PAG and TTT ligands can be applied to a broad range of materials and substrates. Different patterns of NCs capped with $NH_4CS_2N_3$ and PAG^+X^- photoactive ligands are shown in Fig. 2 and figs. S5, S7, and S11. DOLFIN works well for NCs of metals, oxides, semiconductors, and magnetic and light-upconverting (such as $NaYF_4$:Yb, Er@CaF_2) materials (*6*). PAG^+X^- can be also used as an additive to sol-gel precursors (*6*). For example, by adding 5%, by weight, (4-methylthiophenyl) methyl phenyl sulfonium triflate (p-CH_3S-C_6H_4)(CH_3)($C_6H_5^-$)S^+OTf^- [where OTf^- is triflate ($CF_3SO_3^-$)] to a mixture of $In(NO_3)_3$, $Ga(NO_3)_3$, and $Zn(CH_3COO)_2$ in 2-methoxyethanol, we patterned indium gallium zinc oxide (IGZO) layers for transparent transistors (Fig. 2A and fig. S5) (*8*).

We generated these positive patterns by making the areas exposed to light and removing materials from the unexposed regions with a developer solution (such as DMF). Negative patterns can be created by using NCs capped with lyophilic ligands, such as oleate and oleylamine, mixed with (p-CH_3S-C_6H_4) $(C_6H_5)_2S^+OTf^-$ PAG (*6*). After UV exposure, photogenerated protons efficiently attacked lyophilic ligands and replaced them with OTf^- groups (*6*). As a very weak nucleophile, triflate forms an ion pair rather than a covalent bond with metal sites at the NC surface (*5*). As a result, exposed areas become soluble in polar solvents and can be washed away with N-methyformamide (NMF) to form a negative pattern (Fig. 2C and fig. S12). Unexposed NCs retain their lyophilic

[1]Department of Chemistry, University of Chicago, Chicago, IL 60637, USA. [2]James Franck Institute, University of Chicago, Chicago, IL 60637, USA. [3]Center for Nanoscale Materials, Argonne National Laboratory, Argonne, IL 60439, USA.
*Corresponding author. Email: dvtalapin@uchicago.edu

Downloaded from http://science.sciencemag.org/ on August 23, 2017

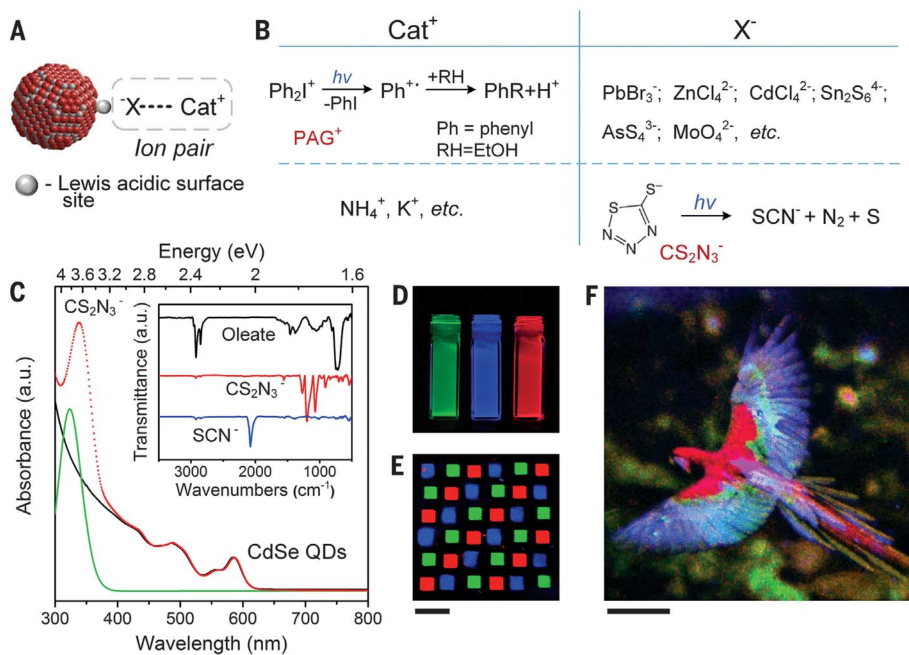

Fig. 1. Optical patterning of nanoparticles with photosensitive inorganic ligands. (**A**) Schematic representation of a nanocrystal with ion pair surface ligands. (**B**) Two complementary approaches to design of photosensitive inorganic ligands. Either cation (PAG^+) or anion [1,2,3,4-thiatriazole-5-thiolate ($CS_2N_3^-$)] of the ion-pair ligand can react under exposure to UV light. (**C**) $CS_2N_3^-$ group has a strong absorption band in the UV region (green line). This UV band is present in the absorption spectra of CdSe NCs capped with $NH_4CS_2N_3$ ligands (red dotted line). An exposure to 254 nm light causes clean transformation of $CS_2N_3^-$ to SCN^- as confirmed by (inset) changes in the IR absorption spectra. (**D**) Colloidal solutions of red-emitting CdSe/ZnS and green-emitting InP/ZnS quantum dots (QDs) and blue-emitting ZnSe/ZnS QDs capped with $NH_4CS_2N_3$ ligands dispersed in DMF. (**E**) Red (R)–, green (G)–, and blue-emitting (B) QDs patterned on SiO_2 substrate by using photoactive $NH_4CS_2N_3$ ligands and 254 nm UV light with a 120 mJ cm^{-2} dose. (**F**) A true-color image containing ~8 × 10^5 RGB subpixels directly photopatterned by use of $CS_2N_3^-$-capped QDs. Scale bars, 5 mm.

surface coats and do not dissolve in NMF. At the same time, the high solubility of PAG in NMF allows us to wash any unreacted PAG from unexposed areas. The patterned layers of organically coated NCs show bright luminescence and can be subjected to various on-film ligand exchange procedures (*4*) so as to optimize charge transport and other properties.

The quality of the patterns was comparable with that achieved with commercial photopolymer resists. Good fidelity is demonstrated in Fig. 3A for the patterns of 10-μm-wide CdSe stripes consecutively patterned on top of each other by using $NH_4CS_2N_3$ ligands; additional images are shown in fig. S13. The edges of patterned regions are sharp and clean (Fig. 3B). The resolution, estimated by using a 1951 U.S. Air Force target, was limited by the one-micrometer mask resolution (Fig. 3C and figs. S14 and S15). The thicknesses of patterned layers are determined by the penetration of UV light into a material. For II-VI and III-V semiconductors, linear absorption coefficients in the UV region level off at ~10^6 cm^{-1} (*9*). In agreement with this estimate, we could efficiently pattern CdTe NC layers with thicknesses between ~10 and 100 nm (Fig. 3D and figs. S8 and S12). Thicker layers can be patterned for materials with low UV absorbance, such as Al_2O_3 and other oxides (fig. S16). Multiple layers of the same or different materials can be photopatterned sequentially with three processing steps per layer: ink coating, exposure, and development (Fig. 3E). Such layer-by-layer patterning permits designing 3D inorganic layers with ~10-nm accuracy along the vertical direction (Fig. 3, F and G). For comparison, layer-by-layer patterning by use of traditional organic photoresists is much less practical for building 3D materials because of a large number of processing steps—typically seven—for patterning each layer (fig. S17) (*3*).

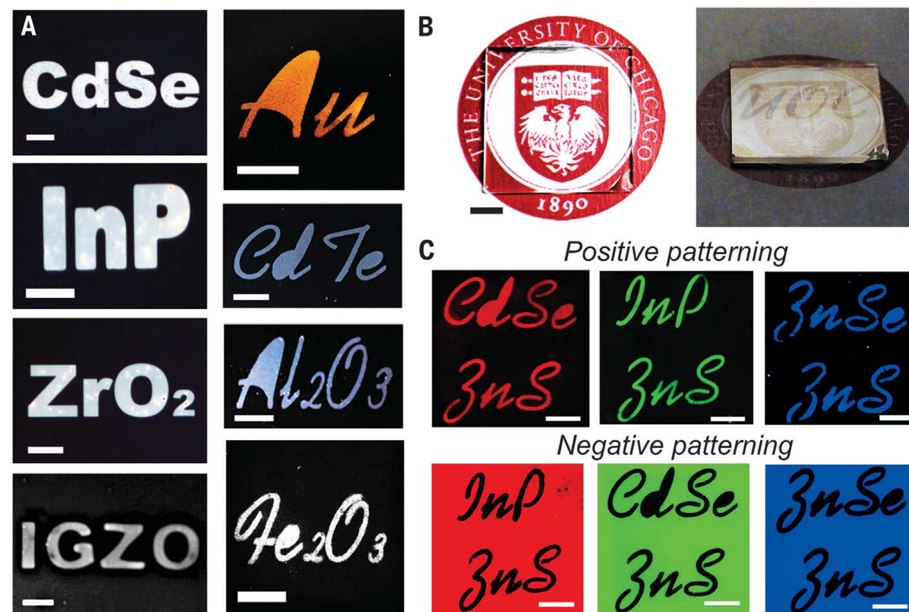

Fig. 2. Examples of optically patterned inorganic materials. (**A**) Different materials patterned by using PAG^+-based ligands (CdTe, ZrO_2, Fe_2O_3, and IGZO) and $CS_2N_3^-$ ligands (CdSe, InP, Au, and Al_2O_3). Scale bars, 100 μm (left column); 5 mm (right column). (**B**) CeO_2 nanocrystals patterned on a glass substrate by using $(Ph_2I)_2MoO_4$ ligands. Scale bar, 5 mm. (**C**) (Top) Positive patterns of CdSe/ZnS (red), InP/ZnS (green), and ZnSe/ZnS (blue) core-shell QDs patterned with $NH_4CS_2N_3$ ligands. (Bottom) Negative patterns of oleate-capped InP/ZnS (red), CdSe/ZnS (green), and ZnSe/ZnS (blue) core-shell QDs patterned by using $(p\text{-}CH_3S\text{-}C_6H_4)(C_6H_5)_2S^+$ OTf^- (OTf, triflate) PAG. Scale bars, 5 mm.

Before this work, NC films were patterned by using traditional photopolymer lithography (*10*), inkjet printing (*11*), and microcontact printing (*12*). Hybrid organic–inorganic composites were patterned by using photochemically active organic ligands (*13*). The ability to optically pattern inorganic phases without diluting them with photopolymers and other organic species is important for practical

Downloaded from http://science.sciencemag.org/ on August 23, 2017

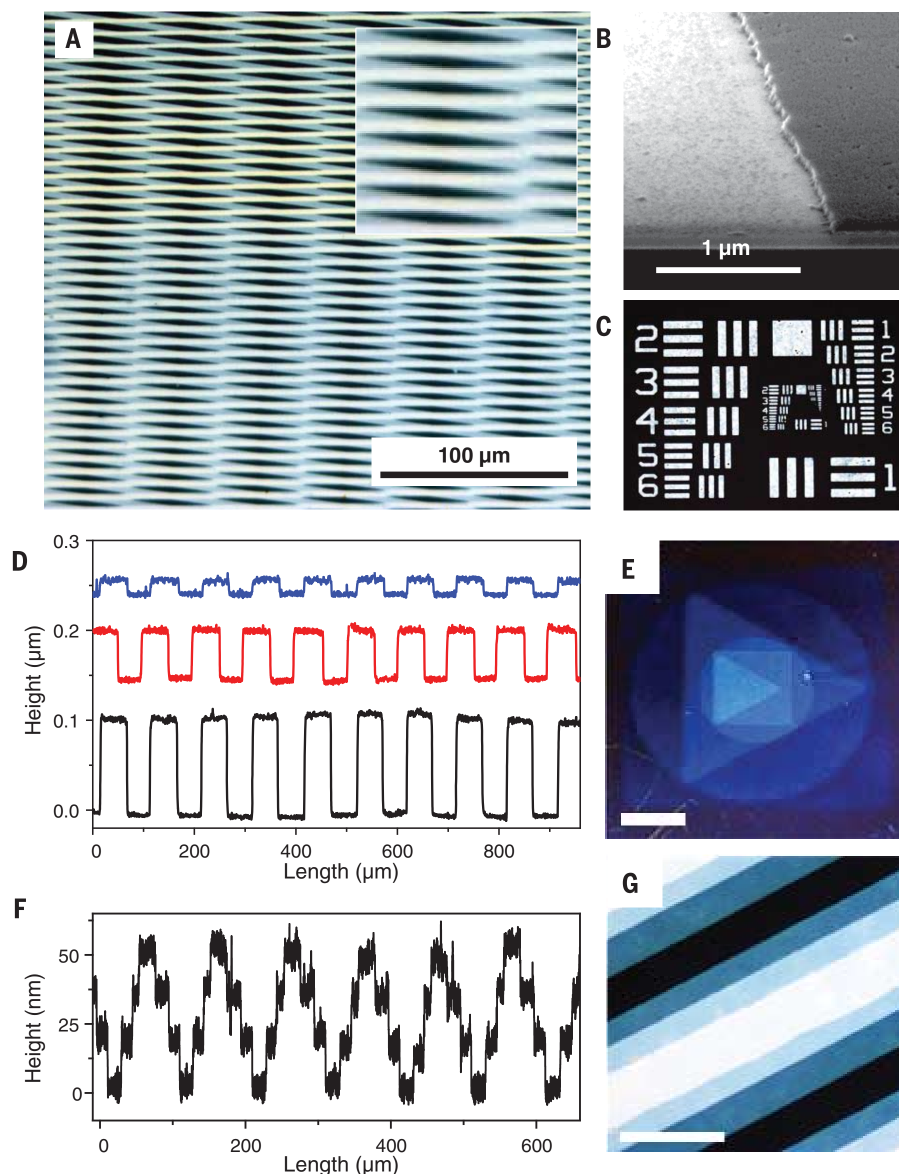

Fig. 3. Typical pattern characteristics. (**A**) A pattern formed by two sequentially defined layers of 10-μm-wide stripes of CdSe NCs patterned by using $NH_4CS_2N_3$ ligands. (Inset) A magnified view of the same pattern. (**B**) SEM image of an edge of a photopatterned layer of CdSe NCs capped with $NH_4CS_2N_3$ ligands. (**C**) 1951 U.S. Air Force target with one-micrometer resolution made of optically patterned CdSe NCs with $NH_4CS_2N_3$ ligands. (**D**) Height profiles of CdTe layers optically patterned by using the NCs capped with $(Ph_2I)_2CdCl_4$ ligands. (**E**) Six layers of ZnSe/ZnS core-shell NCs sequentially patterned by using $NH_4CS_2N_3$ ligands. This three-dimensional pattern was created by using 19 process steps, whereas traditional photopolymer lithography requires 43 process steps (6). Scale bar, 5 mm. (**F** and **G**) Height profile and optical microscopy image of a multilayer stripe pattern created by using CdSe NCs with $NH_4CS_2N_3$ ligands. Scale bar, 50 μm.

applications. A number of recent studies have shown that eliminating organic components from NC films reduces dielectric mismatch and dramatically improves interfacial charge transport (*14*, *15*). Inorganic ligands can also be designed to promote the sintering of NCs into a continuous inorganic layer (*16*). Switching to inorganic surface ligands has resulted in improved performance of solution-processed solar cells (*16*, *17*), photodetectors (*18*), FETs (*19*, *20*), materials for lasing (*21*), and electrochromic windows (*22*).

To evaluate the practical utility of DOLFIN, we characterized the properties of several representative metals, dielectrics, and semiconductors patterned by using photosensitive inorganic ligands. Shown in Fig. 4A is an emission spectrum from red-, green-, and blue-emitting core–shell QDs patterned as an array of square "pixels" (Fig. 1E). The spectrum shows sharp peaks of band-edge emission from the original QDs without apparent signs of core etching or trap emission.

Gold NCs were patterned by using photoactive $NH_4CS_2N_3$ ligands and then annealed at 150°C for 20 min. Resistivity (ρ) of a 60-nm-thick film measured with the four-probe van der Pauw method was 5.2×10^{-8} ohm m at 300 K (fig. S18). This value is comparable with the resistivity of evaporated Au films (*6*), showing that our approach is suitable for direct patterning of metallic electrodes and interconnects. SCN^- ions, formed after UV exposure of TTT ligands, do not impede charge transport and are widely used as conductive inorganic ligands for metal and semiconductor NCs (*23*).

Oxide NCs are used for dielectric layers in electronic circuits and various coatings (*19*). We measured the dielectric properties of Al_2O_3 NC layers patterned by using NH_4TTT ligands. In a flat capacitor configuration, a 125-nm-thick Al_2O_3 film showed a dielectric constant $\varepsilon = 6.9 \pm 0.3$ across a 10^2- to 10^5-Hz frequency range, with a low leakage current corresponding to $\rho > 10^{14}$ ohm cm (Fig. 4B, inset). These ε values agree with predictions from the Bruggeman effective medium theory for a film composed of nanoscale Al_2O_3 grains (*6*) and are slightly lower than ε for dense Al_2O_3 films deposited through atomic layer deposition (ALD; $\varepsilon = 7.7 \pm 0.4$) (*24*). The refractive index (n) of patterned Al_2O_3 films, measured with ellipsometry at 632.8 nm, was 1.40 and can be compared with n = 1.5 to 1.6 for ALD-grown dense Al_2O_3 films. Higher n values were observed for ZrO_2, ZnO, and CeO_2 NC layers (n = 1.62, 1.67, and 1.82, respectively) patterned by using PAG ligands (fig. S19) (*6*). Very similar refractive indices were measured for NC films prepared without photoactive ligands.

The performance of solution-processed semiconductor devices has advanced in recent years, but methods for the integration of these devices into complex circuits have yet to be established. To assess the quality of semiconductor layers patterned by means of DOLFIN, we made prototype FETs (*6*). Their transfer and output characteristics are shown in Fig. 4, C to F, and figs. S20 and S21. Both PAG- and TTT-based photosensitive ligands demonstrated good FET performance. For example, a 30-nm-thick film of CdSe NCs photopatterned with $(Ph_2I)_2CdCl_4$ ligands showed electron mobility (μ_e) of 20 cm^2/V s (fig. S20), which is similar to the values reported for CdSe NCs with structurally related but not photosensitive ligands (*16*). CdSe NCs with compositionally matched $Cd_2Se_3^{2-}$ semiconductor solders (*25*), patterned by using $(p\text{-}CH_3S\text{-}C_6H_4)(C_6H_5)_2S^+OTf^-$ PAG (*6*), enabled FETs with $\mu_e > 100$ cm^2/V s (Fig. 4, C and D). Transparent IGZO films, patterned by using the same PAG, demonstrated robust FETs with μ_e = 4 to 10 cm^2/V s, current modulation $>10^4$, and negligible hysteresis (Fig. 4, E and F, and fig. S21). These numbers are on par with state-of-the-art solution-processed FETs (*1*, *8*, *20*).

The above examples show that PAG- and TTT-based surface ligands enable direct optical patterning of numerous inorganic materials with resolution comparable with that of traditional

Downloaded from http://science.sciencemag.org/ on August 23, 2017

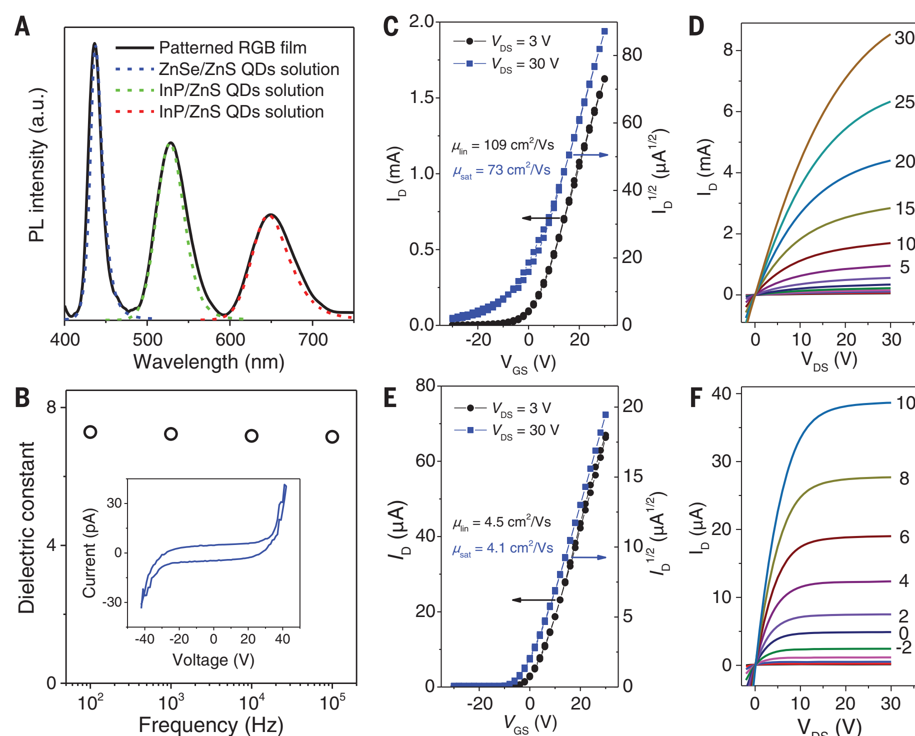

Fig. 4. Properties of directly optically patterned semiconductor and dielectric materials. (**A**) Photoluminescence spectrum of pixels composed of red-, green-, and blue-emitting QDs patterned by using $NH_4CS_2N_3$ ligands. The emission spectra of corresponding QD solutions are shown as dashed lines. The excitation wavelength was 360 nm. (**B**) Dielectric constant of Al_2O_3 layer patterned by using $NH_4CS_2N_3$ ligands. The measurements were carried out for an $Al/Al_2O_3/Al$ flat capacitor with a 125-nm-thick Al_2O_3 layer and an area of 0.64 mm^2. (Inset) A current-voltage relation (*I-V*) characteristic used to measure resistivity of the Al_2O_3 layer. (**C** and **D**) Transfer and output characteristics of an FET with a channel made of compositionally matched $CdSe/Cd_2Se_3^{2-}$ ligands and $CdCl_2$ treatment (*6*). (**E** and **F**) Transfer and output characteristics of a FET with an IGZO channel. The channel length was 30 µm, and the channel width was 180 µm.

photolithography, without compromising the electronic and optical characteristics of patterned materials. We view this approach as an important step toward a broad technological adaption of solution-processed metals, dielectrics, and semiconductors. The compatibility with a broad range of substrates—including silicon, glass, and polymers—provides an avenue for the development of various hybrid devices.

REFERENCES AND NOTES

1. C. R. Kagan, E. Lifshitz, E. H. Sargent, D. V. Talapin, *Science* **353**, aac5523 (2016).
2. Y. Xia, J. A. Rogers, K. E. Paul, G. M. Whitesides, *Chem. Rev.* **99**, 1823–1848 (1999).
3. C. A. Mack, *Fundamental Principles of Optical Lithography* (Wiley, 2007).
4. M. A. Boles, D. Ling, T. Hyeon, D. V. Talapin, *Nat. Mater.* **15**, 141–153 (2016).
5. P. E. Chen, N. C. Anderson, Z. M. Norman, J. S. Owen, *J. Am. Chem. Soc.* **139**, 3227–3236 (2017).
6. Materials and methods are available as supplementary materials.
7. D. H. Webber, R. L. Brutchey, *Dalton Trans.* **41**, 7835–7838 (2012).
8. K. K. Banger *et al.*, *Nat. Mater.* **10**, 45–50 (2011).
9. *Numerical Data and Functional Relationships in Science and Technology, Landolt-Börnstein* (Springer, 1982).
10. J. S. Park *et al.*, *Nano Lett.* **16**, 6946–6953 (2016).
11. E. Tekin *et al.*, *Adv. Funct. Mater.* **17**, 23–28 (2007).
12. G. J. Supran *et al.*, *MRS Bull.* **38**, 703–711 (2013).
13. W. J. Kim *et al.*, *Nano Lett.* **8**, 3262–3265 (2008).
14. C. R. Kagan, C. B. Murray, *Nat. Nanotechnol.* **10**, 1013–1026 (2015).
15. M. V. Kovalenko, M. Scheele, D. V. Talapin, *Science* **324**, 1417–1420 (2009).
16. H. Zhang, J. M. Kurley, J. C. Russell, J. Jang, D. V. Talapin, *J. Am. Chem. Soc.* **138**, 7464–7467 (2016).
17. M. Liu *et al.*, *Nat. Mater.* **16**, 258–263 (2017).
18. E. Lhuillier, S. Keuleyan, P. Zolotavin, P. Guyot-Sionnest, *Adv. Mater.* **25**, 137–141 (2013).
19. J. H. Choi *et al.*, *Science* **352**, 205–208 (2016).
20. J. Jang *et al.*, *Nano Lett.* **15**, 6309–6317 (2015).
21. M. M. Adachi *et al.*, *Nat. Commun.* **6**, 8694 (2015).
22. A. Llordés, G. Garcia, J. Gazquez, D. J. Milliron, *Nature* **500**, 323–326 (2013).
23. A. T. Fafarman *et al.*, *J. Am. Chem. Soc.* **133**, 15753–15761 (2011).
24. M. D. Groner, F. H. Fabreguette, J. W. Elam, S. M. George, *Chem. Mater.* **16**, 639–645 (2004).
25. D. S. Dolzhnikov *et al.*, *Science* **347**, 425–428 (2015).

ACKNOWLEDGMENTS

We thank N. Ludwig for help with image analysis; A. Filatov for x-ray diffraction analysis; M. Hudson for providing selenocadmate ligands; and B. Tian, J. Park, V. Srivastava, and T. Shpigel for reading the manuscript. The work was supported by the U.S. Department of Defense Air Force Office of Scientific Research under grant FA9550-14-1-0367, NSF under award CHE-1611331, NSF Materials Research Science and Engineering Center Program under award DMR-1420709, and the II-VI Foundation. Use of the Center for Nanoscale Materials was supported by the U.S. Department of Energy, Office of Science, Office of Basic Energy Sciences, under contract DE-AC02-06CH11357. Data supporting the findings of this study are available within the article and the supplementary materials and from the corresponding authors upon reasonable request. The quantum dot samples can be provided by the authors under a materials transfer agreement with the university. Y.W., H.Z., and D.V.T. are inventors on patent application U.S. 62/486,566 submitted by the University of Chicago that covers nanocrystal patterning chemistry and methods.

SUPPLEMENTARY MATERIALS

www.sciencemag.org/content/357/6349/385/suppl/DC1
Materials and Methods
Figs. S1 to S21
Tables S1 to S4
References (*26*–*51*)

23 March 2017; accepted 27 June 2017
10.1126/science.aan2958

Downloaded from http://science.sciencemag.org/ on August 23, 2017

Science

Direct optical lithography of functional inorganic nanomaterials

Yuanyuan Wang, Igor Fedin, Hao Zhang and Dmitri V. Talapin

Science **357** (6349), 385-388.
DOI: 10.1126/science.aan2958

Patterning without polymers

Nanoscale patterning usually requires multiple steps to mask, pattern, and develop sequential layers. One overriding concern is to obtain compatibility between all the materials, as well as the patterning techniques used, to ensure accurate and clean processing. Wang *et al.* use light-responsive ligands to change the solubility of nanocrystals in specific solvents, so that development can be done by simple redispersion of nanocrystals in dark regions (see the Perspective by Striccoli). The process can fully utilize the advantages of conventional semiconductor processing, but without the need for photoresists, because the nanocrystals are only deposited where they are exposed to light.

Science, this issue p. 385; see also p. 353

ARTICLE TOOLS http://science.sciencemag.org/content/357/6349/385

SUPPLEMENTARY MATERIALS http://science.sciencemag.org/content/suppl/2017/07/27/357.6349.385.DC1

RELATED CONTENT http://science.sciencemag.org/content/sci/357/6349/353.full

REFERENCES This article cites 48 articles, 4 of which you can access for free
http://science.sciencemag.org/content/357/6349/385#BIBL

PERMISSIONS http://www.sciencemag.org/help/reprints-and-permissions

Use of this article is subject to the Terms of Service

Science (print ISSN 0036-8075; online ISSN 1095-9203) is published by the American Association for the Advancement of Science, 1200 New York Avenue NW, Washington, DC 20005. 2017 © The Authors, some rights reserved; exclusive licensee American Association for the Advancement of Science. No claim to original U.S. Government Works. The title *Science* is a registered trademark of AAAS.

Downloaded from http://science.sciencemag.org/ on August 23, 2017